NMR Analysis of Structure and Dynamics of the Cytosolic Tails of Integrin αIIbβ3 in Aqueous Solution†

Tobias S. Ulmer,‡ Brian Yaspan,§ Mark H. Ginsberg,*,§ and Iain D. Campbell*,‡,||

Department of Biochemistry, University of Oxford, South Parks Road, Oxford, OX1 3QU, U.K., Department of Vascular Biology, The Scripps Research Institute, La Jolla, CA 92037, and Oxford Centre for Molecular Sciences, South Parks Road, Oxford OX1 3QT, U.K.

Received February 16, 2001; Revised Manuscript Received April 2, 2001

ABSTRACT: The structural and dynamic properties of the cytosolic tails of the adhesion receptor integrin αIIbβ3, fused to a coiled-coil construct via $(Gly)_3$ linkers, were studied in aqueous solution by nuclear magnetic resonance (NMR) spectroscopy. Both tails were largely flexible and unstructured, although, in the β3 tail, residues Arg^{724}−Ala^{735} have a propensity to form a helical structure and residues Asn^{744}−Tyr^{747} (NPLY) have a propensity to adopt reverse-turn conformations. The mutation β3(Y747A) disrupted this reverse-turn tendency and markedly reduced the affinity of the head domain of the cytoskeletal protein, talin for the β3 tail. Omission of the $(Gly)_3$ linker connecting the coiled-coiled helices and the integrin tails lead to helix propagation into the β3 tail extending up to eight residues. A variety of different tail constructs were made and studied to reveal tail−tail interactions, but surprisingly no significant interactions between both tails could be detected within the context of our constructs. These results provide structural insight into a highly conserved β tail motif (NPXY/F) required for integrin signaling and highlight a second transiently structured region (residues Arg^{724}−Ala^{735}), which might also be of functional significance.

Integrin adhesion receptors are heterodimers of α- and β-subunits that contain a large extracellular domain responsible for ligand binding, a single transmembrane domain, and a cytoplasmic domain that, in most cases, consists of 20−70 amino acid residues (*1*, *2*). Integrins play important roles in cell adhesion, cell migration and control of cell differentiation, proliferation, and programmed cell death. They mediate bidirectional signal transduction across the plasma membrane. Binding of ligands to integrins transmits signals into the cell and results in cytoskeletal reorganization, gene expression, and cellular differentiation (outside-in signaling). Conversely, signals from within the cell can also propagate through integrins and alter integrin ligand-binding affinity and cell adhesion (inside-out signaling) (*3*). The cytoplasmic domains of integrins play a pivotal role in these bidirectional signaling processes, and intensive efforts have focused on identifying interactions of these domains (*4*−*6*). Mutations or truncations of specific membrane-distal sequences in β cytoplasmic tails can disrupt integrin-triggered signaling and cytoskeletal organization (*7*−*15*). A particularly sensitive site is a highly conserved NPXY/F motif in the β cytoplasmic domain. Furthermore, overexpression of isolated β cytoplasmic tail chimeras can profoundly suppress both inside out and outside-in signaling, possibly by titration of critical regulatory molecules (*16*−*18*), and mutation of the NPXY/F motif can abolish this activity (*19*). Conversely, when clustered or highly overexpressed, these β tail chimeras can themselves generate some of the biochemical signals, such as tyrosine phosphorylation of FAK, usually triggered by integrin ligation (*17*, *18*), and this signaling is also dependent on the NPXY/F motif (*20*). The roles of the α cytoplasmic tails seem even more complex. For example, deletion of certain membrane-distal α tail sequences can result in constitutive biochemical signaling (*21*) and at the same time lead to reduced cell adhesion possibly by inappropriately tethering the integrin (*22*−*24*). Thus, α tails exert both positive and negative influences and an NPXY/F motif in the β tail is essential for normal integrin signaling.

Studies of platelet integrin αIIbβ3 have suggested that integrin α and β cytoplasmic tails might interact in vivo and in vitro. An in vivo charge swapping mutation study suggested that the αIIb and β3 tails have a direct site of interaction between αIIb(R995) and β3(D723) (*25*). In aqueous solution, circular dichroism (CD) studies showed that isolated αIIb, β3, and αIIb + β3 peptides or constructs corresponding to αIIb + β3 are largely unfolded (*26*−*28*). However, when the two peptides were mixed, changes in CD spectra and intrinsic fluorescence also suggested in vitro interactions (*27*). Surface plasmon resonance analysis indicated an interaction of immobilized β3 tail with soluble αIIb tail in the micromolar range (*29*). The tails in nonaqueous solution or the myristoylated αIIb tail in DPC micelle solution exhibit more defined 3D[1] structures (*28*, *30*, *31*). A 3D structure of the myristoylated αIIb in DPC micelle

† T.S.U. acknowledges support from the German Academic Exchange Service (DAAD) and BBSRC. M.H.G. was supported by grants from the NIH. I.D.C. acknowledges support from the Wellcome Trust and, through the Oxford Centre for Molecular Sciences, from MRC, BBSRC, and EPSRC. This is Scripps Publication Number 13928-VB.

‡ Department of Biochemistry, University of Oxford.

§ The Scripps Research Institute.

|| Oxford Centre for Molecular Sciences.

* To whom correspondence should be addressed. M.H.G. Telephone: 1-858-784-7124. Fax: 1-858-784-7343. E-mail: ginsberg@scripps.edu; I.D.C. Telephone: +44-(0)1865-275346. Fax: +44-(0)-1865-275253. E-mail: idc@bioch.ox.ac.uk.

10.1021/bi010338l CCC: $20.00
Published on Web 05/30/2001

solution was determined (*30*) as well as a 3D structure of the αIIb tail in 45% TFE solution (*31*). However, to date, there has been no NMR analysis of the β3 cytoplasmic domain or of its potential interactions with the αIIb tail in aqueous solutions.

The current study characterizes the cytosolic tails of integrin αIIbβ3, and their putative interaction in aqueous solution using a coiled-coil construct that has been introduced previously (*26*, *32*). It is used here, in an improved form, in a nuclear magnetic resonance (NMR) study. We found that the tails were globally unfolded in aqueous solution. However, the β3 tail had a distinct helical propensity for residues $Arg^{724}-Ala^{735}$ and a strong reverse-turn propensity at the NPLY motif. Mutation of this motif markedly reduced the affinity of the head domain of the cytoskeletal protein, talin. That mutation also disrupted the reverse-turn and led to a somewhat reduced helical propensity in the membrane proximal region (residues $Arg^{724}-Ala^{735}$). Omission of the $(Gly)_3$ linker connecting the coiled-coiled helices and the integrin tails leads to helix propagation into the β3 tail extending up to eight residues. Surprisingly, no significant interactions between the αIIb and β3 tails could be detected within the context of our construct. These results provide a structural insight into a highly conserved β tail motif required for integrin signaling and highlights a second transiently structured region (residues $Arg^{724}-Ala^{735}$), which might have functional significance as well.

EXPERIMENTAL PROCEDURES

Protein Production and Purification. Polymerase chain reaction (PCR) as described (*32*) was used to create a cDNA encoding the modified GCN4 heptad repeat protein sequences reported by John et al. (*33*). In one form, Lys residues at the g1 and e2 positions of the heptad repeats render the helix "Jun-like." Alternatively, Glu substitutions at these positions result in a "Fos-like" helix (Figure 1A) that preferentially forms heterodimers with the "Jun-like" helix (*33*). A variable number of Gly residues (0−4) were added to the c-terminus of heptad repeats to modify the potential of the α-helical coiled-coils to induce structure in the integrin cytoplasmic domains (*32*) and to vary the stagger of the integrin tails relative to each other. The cDNAs were ligated into an *Nde*I−*Hin*dIII-restricted modified pET15b vector (*32*) (Novagen).

αIIb and β3 integrin cytoplasmic domain cDNAs were generated by PCR from appropriate cDNAs using forward oligonucleotides introducing a 5′-*Hin*d III site and reverse oligonucleotide creating a 3′-*Bam*HI site directly after the stop-codon. Integrin cytoplasmic domains were joined to the helix as *Hin*dIII−*Bam*HI fragments and verified by sequencing (Figure 1). The identity of each model protein is specified by the nature of the GCN4 helix (Jun-like = J, Fos-like = F), the number of Gly spacers (G0−4), and the identity of the integrin tail (αIIb, β3) e.g., JG3αIIb.

Recombinant proteins were expressed in BL21(DE3)pLysS cells (Novagen) and purified as described with an additional final purification step on a reverse phase HPLC column (Vydac) (*32*). To isotopically label model proteins with ^{15}N, the BL21 cells were cultured in M9 minimal medium containing 20 mM $^{15}NH_4Cl$ (Isotec) as the sole nitrogen source. To form heterodimers, a mixture of 45 μM β3 and 90 μM αIIb cytoplasmic tail model proteins were denatured for 20 min at 100 °C in the presence of 10 mM dithiothreitol (DTT). The DTT was removed by gel filtration through a PD10 column (Biorad), and the mixture was then air-oxidized by stirring overnight. The disulfide-bonded products were purified by reverse phase C18 HPLC. Products were analyzed by electrospray ionization mass spectrometry using an API-III quadrupole spectrometer (Sciex), and masses varied by less than 0.1% from expected masses (Table 1). The increase in mass of the ^{15}N-labeled subunits indicated ≥91% incorporation of ^{15}N.

Peptide Synthesis. The "αIIb" peptide containing a Val^{990}−Leu substitution, KLGFFKRNRP PLEEDDEEGQ, was synthesized by the Oxford Centre for Molecular Sciences peptide synthesis facility. A "wild-type" αIIb cytoplasmic domain peptide, KVGFFKRNRP PLEEDDEEGQ, was synthesized in the Microchemistry core at the Scripps Research Institute. The C-terminus of the αIIb peptide was a Gln residue because the encoded Glu residue is reported to be amidated in the native receptor (*34*). All peptides were synthesized with a free C-terminal carboxyl group.

NMR Sample Preparation. NMR samples at pH 4.5 were prepared by dissolving freeze-dried protein in 93.3% 10 mM acetic acid-d_4, pH 4.5/6.7% D_2O, adjusting the pH to 4.5 by addition of NaOH and HCl and exchanging the buffer by four ultrafiltration and dilution cycles. The following samples were prepared at pH 4.5 (cf. also Table 2): 1.2 mM JG3αIIb, ^{15}N-FG3β3; 1.2 mM JG3αT, ^{15}N-FG3β3; 1.2 mM ^{15}N-FG3β3, ^{15}N-FG3β3; 1.2 mM JG3αT, ^{15}N-FG3β3(Y747A); 1.2 mM JG0αIIb, ^{15}N-FG0β3 and 0.8 mM ^{15}N-JG3αIIb, FG3β3; 0.8 mM ^{15}N-JG3αIIb, JG3αT; 0.8 mM ^{15}N-JG3αIIb, ^{15}N-JG3αIIb. Samples at pH 6.8 were prepared by dissolving freeze-dried protein in 95% 20 mM phosphate buffer, pH 6.8, 120 mM NaCl/5% D_2O or, alternatively, in 95% 50 mM Tris-d_{11}/HCl, pH 6.8, 100 mM NaCl, with and without 5 mM $CaCl_2$/5% D_2O, readjusting the pH with NaOH and HCl and exchanging the buffer by four ultrafiltration and dilution cycles. Samples at pH 7.4 were prepared by readjusting the pH from pH 6.8 with NaOH and HCl. At pH 6.8, the following samples were prepared: 0.6 mM JG3αIIb, ^{15}N-FG3β3, 0.6 mM ^{15}N-JG3αIIb, FG3β3, 0.6 mM JG4αIIb, ^{15}N-FG3β3, 0.6 mM JG1αIIb, ^{15}N-FG3β3, 0.6 mM JG2αIIb, ^{15}N-FG3β3, 0.6 mM JG3αIIb, ^{15}N-FG1β3, 0.6 mM J, ^{15}N-FG3β3 and (without the ultrafiltration step) 0.6 mM J, ^{15}N-FG3β3 + 1.2 mM αIIb peptide. At pH 7.4, the following samples were prepared: 0.6 mM J, ^{15}N-FG3β3 and 0.6 mM J, ^{15}N-FG3β3 + 1.2 mM αIIb peptide. Small quantities of dioxane were added as chemical shift reference.

NMR Spectroscopy. All the NMR experiments were performed at 37 °C (unless otherwise stated) on spectrometers operating at ^1H frequencies of 500, 600, and 750 MHz. Backbone assignment of subunits FG3β3; FG3β3(Y747A); FG0β3; and JG3αIIb in the respective model proteins (cf. NMR sample preparation) at pH 4.5 was achieved using a combination of 2D ^{15}N-^1H HSQC (*35*, *36*), 3D TOCSY-

[1] Abbreviations: 2D and 3D, two- and three-dimensional; CD, circular dichroism; HMQC, heteronuclear multiple-quantum correlation; HSQC, heteronuclear single-quantum correlation; ITC, isothermal titration calorimetry; K_D, dissociation constant; NMR, nuclear magnetic resonance; NOE, nuclear Overhauser enhancement; NOESY, nuclear Overhauser enhancement and exchange spectroscopy; ppm, parts per million; TFE, trifluoroethanol; TOCSY, total correlation spectroscopy; $^3J_{HN\alpha}$, scalar coupling constant between H^N and Hα.

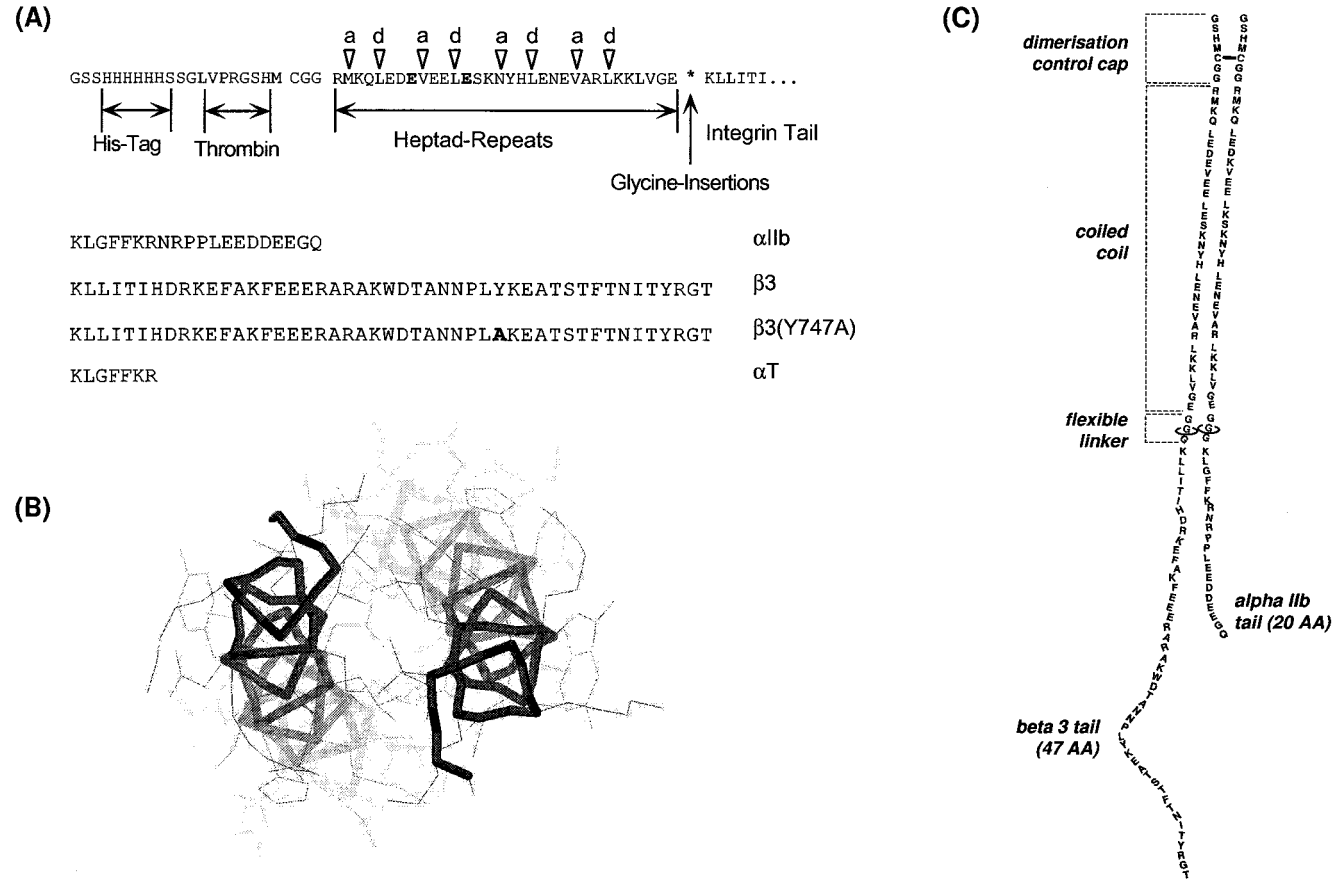

FIGURE 1: Integrin cytoplasmic domain mimics. (A) Strategy. Depicted is the amino acid sequence of the recombinant mini-subunit. An N-terminal His-Tag is used to immobilize and purify the construct. A thrombin cleavage site allows release of the His-Tag, and a single cysteine is used to form covalent parallel dimers in a defined vertical stagger. Heptad repeats, from GCN4, nucleate the formation of a parallel dimeric coiled-coil. The presence of Glu residues at the g1 and e2 positions of the heptad repeats (bold face) render the helix "Fos-like". Lys substitutions at this position result in a "Jun-like" helix that preferentially forms heterodimers with the "Fos-like" helix (*33*). Cytoplasmic domains, such as that of integrin αIIbβ3 depicted here, were joined to the coiled-coil. Variable numbers of Gly residues were inserted between the coiled-coil and the integrin tail to disrupt induced helical structure in the cytoplasmic domain (*32*) and vary the stagger of the tails. Below is a list of the integrin-specific sequences of all recombinant constructs used in this study. All integrin peptides correspond to published human integrin sequences (as cited in the text). To preserve a *Hin*dIII site, a Val residue in the cytoplasmic domain of the human integrin αIIb chain was replaced by Leu. αT represents an αIIb cytoplasmic domain truncation that unmasks the signaling (*21*) and cytoskeletal targeting (*13*) activities of the β3 subunit. (B) GCN4 structure. Bottom view of the crystal structure of the coiled-coil part of the yeast transcription factor GCN4 (*70*) used for attachment of integrin tails. The crystal structure does not show the last two coiled-coil residues, ER, because of helix fraying at the C-terminus. In our model construct, the coiled-coil is terminated with E and a variable number of Gly residues. The axial, lateral, and vertical orientation of the tails will depend the lengths of the Gly spacers. (C) Schematic representation of a JG3αIIb-FG3β3 model protein mimic of the cytosolic face of integrin αIIbβ3. The heterodimeric model protein was formed from a Jun-like αIIb and Fos-like β3 mini-subunit each containing a three Gly spacer. The polyhistidine tag was removed from the subunits to facilitate NMR analysis. The integrin tails were fused to the coiled-coil derived from the yeast transcription factor GCN4 via a $(Gly)_3$ linker. The coiled-coil is covalently linked by a disulfide bridge at the N-terminus.

HSQC (*37*, *38*), and 3D NOESY-HSQC (*39*). A mixing time of ~40 ms was used for TOCSY and mixing times of 175 and 300 ms were used for NOESY. Acquisition times were typically 169.1 ms (t_1), 102.4 ms (t_2) for 2D and 21.9 ms (t_1), 52.6 ms (t_2), 102.4 ms (t_3) for 3D. The acquisition time in the direct ^{1}H dimension was limited by H^N-Hα coupling. Experiments at 30 °C were used to resolve some overlapping peaks and also to reduce amide proton solvent chemical exchange at pH 6.8 and 7.4. Chemical shifts at pH 6.8 and 7.4 were very similar to pH 4.5. Data were processed with Felix 2.3 (Biosym Inc., San Diego, CA) and analyzed with XEasy (*40*).

Transverse (^{15}N-T_2) relaxation times and the heteronuclear steady-state ^{15}N-{^{1}H} NOE were measured at 60.8 MHz using procedures as described in refs *41* and *42*. Transverse relaxation time constants (T_2) were measured using a spin−echo sequence with a CPMG delay of 500 μs. Chemical shift anisotropy (CSA) and dipolar cross-correlation was removed by application of proton 180° pulses in the middle of the basic CPMG block (*43*, *44*). ^{1}H-saturation in the NOE experiment was effected by means of a train of 120° flip-angle pulses at 10 ms intervals for 5 s. The T_2 and ^{15}N-{^{1}H} NOE spectra were processed with mild resolution enhancement to optimize resolution while maintaining a good signal-to-noise ratio. Relaxation rates were derived from two-parameter exponential fits to the resonance intensities (*45*). The heteronuclear NOE was calculated as the ratio of resonance intensities in the spectra recorded with and without saturation.

$^3J_{HN\alpha}$ coupling constants were measured from 2D ^{15}N-^{1}H HMQC-*J* experiments (*46*, *47*) recorded at a ^{1}H frequency of 750 MHz. Acquisition times were 300.6 ms (t_1) and 102.4

Table 1: Characterization of Model Protein Mini-Subunits[a]

model protein subunit	expected mass	measured mass (± SEM)
J G3 αT	7284.2	7285 ± 1.6
J G0 αIIb	8622.6	8624 ± 1.2
J G1 αIIb	8679.6	8681 ± 1.1
J G2 αIIb	8736.7	8737 ± 1.7
J G3 αIIb	8793.8	8794 ±1.0
J G4 αIIb	8850.8	8854 ± 1.3
F G0 β3	11796.1	11797 ± 1.7
F G1 β3	11853.2	11855 ± 2.3
F G3 β3	11967.3	11969 ± 3.9
F G3 β3 (Y747A)	11875.3	11880 ± 1.0

[a] Each model protein subunit was comprised of a GCN4 helix that was either Jun-like (J) or Fos-like (F) joined via a variable Gly (G0-4) spacer to an integrin (αT, αIIb, β3, β3(Y747A)) tail. Expected masses were predicted from the desired covalent structure and did not account for natural abundance of stable isotopes, e.g., ^{13}C. Measured masses were determined by electrospray ionization mass spectroscopy.

Table 2: Overview of the αIIbβ3 Model Proteins and ^{15}N Labeling Used[a]

Basic constructs	
a. JG3αIIb, ^{15}N-FG3β3	b. ^{15}N-JG3αIIb, FG3β3
Probing tail−tail interactions	
c. JG3αT, ^{15}N-FG3β3	d. JG3αT, ^{15}N-JG3αIIb
e. ^{15}N-FG3β3, ^{15}N-FG3β3	f. ^{15}N-JG3αIIb, ^{15}N-JG3αIIb
Implications of the GCN4 coiled-coil	
g. J, ^{15}N-FG3β3 ± free αIIb peptide	h. JG0αIIb, ^{15}N-FG0β3
Disruption of the NPLY motif	
i. JG3αT, ^{15}N-FG3β3(Y747A)	
Stagger variation	
j. JG4αIIb, ^{15}N-FG3β3 (+1)[b]	k. JG2αIIb, ^{15}N-FG3β3 (−1)[b]
l. JG1αIIb, ^{15}N-FG3β3 (−2)[b]	m. JG3αIIb, ^{15}N-FG1β3 (+2)[b]

[a] Each model protein subunit was comprised of a GCN4 helix that was either Jun-like (J) or Fos-like (F) joined via a variable Gly (G0−4) spacer to an integrin (αT, αIIb, β3, β3(Y747A)) tail. [b] Indicates the number of residues by which the vertical tail−tail stagger was shifted through variation of the Gly spacer length.

ms (t_2). The final digital resolution in F_1 was 0.42 Hz. Cross-sections parallel to F_1 through HMQC-*J* cross-peaks were fitted for nonglycine residues to in-phase Lorentzian doublets in which both components have different line width by optimization of the coupling constant and line widths (*48*). A shifted (30°) sine-bell window was applied in t_1 and to the simulated in-phase Lorentzian doublet.

Affinity Chromatography. A glutathione *S*-transferase (GST) recombinant talin head domain (residues 1−435 of talin) fusion protein was expressed and purified (*49*). Binding of recombinant talin head domain to JG3αT-FG3β3 or JG3αT-FG3β3(Y747A) model proteins was measured as described (*32*, *49*). Briefly, the model proteins were immobilized via their polyhistidine tags on His-Bind Ni^{2+} chelate resin (Novagen) according to the manufacturer's instructions. Varying concentrations of head domain in buffer X (10 mM PIPES, 50 mM NaCl, 150 mM sucrose, 50 mM NaF, and 40 mM $Na_4P_2O_7$, pH 6.8) were added to 100 μL of a 5% slurry of the model protein-coated resin. After 1 h, incubation at room temperature, with continuous shaking, the resin was washed 5 times with buffer X, and bound proteins were eluted by boiling in 15 μL of SDS sample buffer containing 10 mM dithiothreitol. Bound proteins were fractionated by 4−20% SDS−PAGE and bound talin head domain was visualized by Coomassie Blue staining and quantified by scanning densitometry.

Isothermal Titration Calorimetry. Titrations were performed at 25 °C with a VP-ITC microcalorimeter (MicroCal Inc., Northampton, MA). The stirred cell contained 1.4 mL J, FG3β3 at 0.07 mM, and the syringe contained 1.26 mM αIIb peptide each in 20 mM Tris/HCl, pH 7.4, 120 mM NaCl, and 5 mM $CaCl_2$. After an initial injection of 2 μL, 26 injections of 5 μL each were performed at 180-s intervals. Blank titrations of αIIb peptide into buffer alone were also performed to correct for heats of dilution and mixing.

RESULTS

The first charged residue after the predicted transmembrane region of each integrin subunit was taken as the beginning of each cytosolic tail, Lys^{989} for αIIb and Lys^{716} for β3, giving a 20-residue long αIIb tail and a 47-residue long β3 tail (Figure 1A). In the majority of the experiments described here, the structure of the tails was studied when connected to heptad repeat sequences (Figure 1A), which form parallel coiled-coils (Figure 1B) in place of the integrin transmembrane domains (*32*). Use of the coiled-coil construct has some clear advantages in simulating the disposition of the tails in intact integrins. The solubility of the β3 tail is much higher than in the free form, and any potential interaction between the αIIb and β3 tails should be enhanced, as intramolecular rather than intermolecular (i.e., entropically less costly) interactions are possible. Potential disadvantages are that the coiled-coil will also affect the axial and lateral orientation of the tails, as well as the vertical orientation (Figure 1B). This potential problem was investigated by introducing a variable glycine linker between the coiled-coil and the tails (Figure 1A,C). Propagation of helix from the coiled-coil into the tails upon omitting the glycine linker was also used to simulate propagation of transmembrane helix into the integrin tails. To fully characterize the αIIbβ3 system, the properties of a large number of different constructs were compared (Table 2). With the exception of possible interactions of the tails with the phospholipid bilayer, potential interactions between the tails and helix propagation can be studied with our constructs. A $(Gly)_3$ linker between the coiled-coil and the tails (Figure 1A,C) proved useful to separate both realms and this basic construct (Table 2a,b) will be discussed first, followed by the structural and functional implications of the β3(Y747A) mutation, the amount of helix propagation into β3 that can be achieved by omitting the $(Gly)_3$ linker, and the search for tail−tail interactions.

Characterization of the Model Protein of αIIbβ3. To reduce the complexity of all NMR spectra either the αIIb or β3 subunit of the model protein (Figure 1C) were selectively labeled with ^{15}N (Table 2a,b). Backbone assignments at pH 4.5 were achieved from 3D NOESY- and TOCSY-HSQC spectra. ^1H-^1H NOEs in the coiled-coil were characteristic for helical secondary structure (*50*). Only sequential ^1H-^1H NOEs were observed in the tails (at the protein concentrations used), characteristic of unstructured proteins (data not shown). The backbone shifts of the canonical GCN4 coiled-coil (Figure 2B) were very similar to the published shifts of GCN4 (*51*). The ^{15}N integrin tail shifts (Figure 2A,B) tally with predicted random-coil shifts (*52*) within 2 ppm. Backbone chemical shifts were very similar in the two examined, accessible pH ranges (pH 7.4−6.8 and 4.8−3.8, e.g., Figures 2 and 6) and indicate equivalent structural properties over this pH ranges. To minimize amide proton

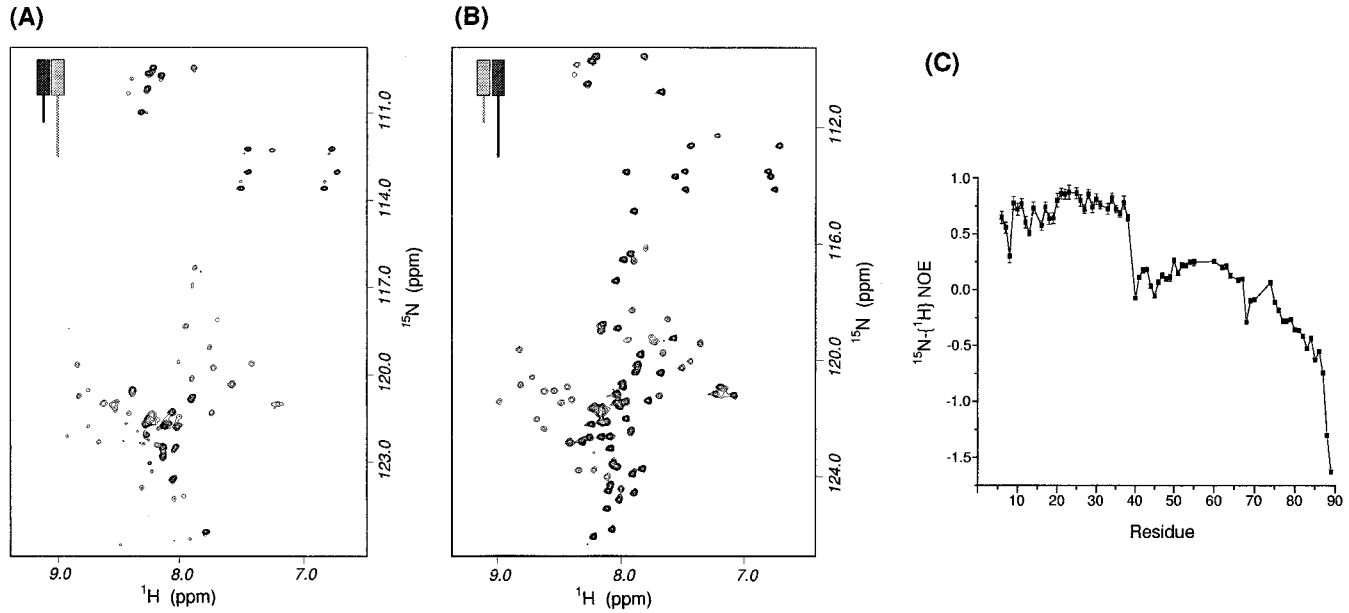

FIGURE 2: $^{1}H^{N}$-^{15}N correlation (HSQC) spectra of the $(Gly)_3$-linked αIIbβ3 model protein in 10 mM acetic acid-d_3 pH 4.5 at 37 °C and 750 MHz. The (A) αIIb and (B) β3 tail, respectively, were individually ^{15}N labeled to reduce spectral complexity. In this type of spectra, each H^N-N group of each amino acid residue gives rise to one signal, side chain NH_x groups can give rise to signals as well. The relatively weak signals in the spectra correspond to coiled-coil residues, while the intense signals correspond to integrin tail residues. The weak signals have chemical shifts characteristic of well-folded structures, while the intense signals have random-coil chemical shifts. (C) ^{15}N-{^{1}H} NOE plot of the $(Gly)_3$-linked αIIbβ3 construct ^{15}N labeled on the β3 tail (Table 2a) at 60.8 MHz in 10 mM acetic acid-d_3 pH 4.5, 37 °C. The ^{15}N-{^{1}H} NOE of each H^N-N group of each amino acid residue reflect local protein backbone order. The folded and unfolded nature of the coiled-coil and the β3 tail, respectively, are apparent. The $(Gly)_3$ linker can be seen to be effective in separating the behavior of both realms.

chemical exchange with solvent water and to maintain Asp and Glu side-chains (pK_a 3.90 and 4.07, respectively) mainly in their deprotonated state, pH 4.5, was chosen to obtain most of the structural and dynamical NMR parameters.

The chemical shift depends directly on the (ensemble of) protein conformation(s) in a sensitive, but complicated manner (*53*), with relative shift changes being, generally, easier to interpret than absolute values. The ^{1}H and ^{15}N backbone chemical shifts of resonances from the coiled-coil region deviate significantly from the tabulated or predicted random-coil shifts (*50*, *52*), while the shifts of the integrin tail region are in close agreement with the random coil values. Taken together with the observed ^{1}H-^{1}H NOE pattern discussed above, these results show that the coiled-coil takes up the expected 3D structure (Figure 1B), while the integrin tails are globally unstructured with a range of conformations.

To further characterize the tails, the $^{3}J_{HN\alpha}$ coupling constant and the ^{15}N-{^{1}H} NOE of each residue was measured. $^{3}J_{HN\alpha}$ is directly related to the angle between H^N-N and Hα-Cα (the torsion angle ϕ) and this angle is directly related to helical or extended backbone conformations (*50*). Individual amino acids have different intrinsic propensities to form helical or extended conformations (*54*) and predicted random-coil $^{3}J_{HN\alpha}$ coupling constants have been compiled to account for this and to serve as a reference (*55*, *56*). The ^{15}N-{^{1}H} NOE is highly sensitive to nano- to picosecond movements of each H^N-N bond vector and can be viewed as a parameter that reflects the degree of backbone order. High ^{15}N-{^{1}H} NOEs are characteristic of well-folded structures (for example, the coiled-coil region); low values are characteristic of unfolded structures such as the integrin tails. Figure 2C illustrates this for the FG3β3 subunit. The $(Gly)_3$ linker can be seen to be effective in separating the behavior of both realms. Regions with significant transient structure should therefore exhibit $^{3}J_{HN\alpha}$ coupling constants that deviate from the predicted random-coil values and have relatively high ^{15}N-{^{1}H} NOEs. Figure 3 compares these parameters for the integrin tail region. High ^{15}N-{^{1}H} NOEs can also arise from hydrophobic clustering (*57*) thus a Kyte & Doolittle hydrophobicity plot (*58*) is also given. For the αIIb tail the ^{15}N-{^{1}H} NOEs are almost all uniformly low (Figure 3A), due to very fast motions of the C-terminus of the peptide they are lowest there. At the N-terminus, the relatively high NOEs around Lys^{989} might still be due to the proximity to the well-folded coiled-coil. The measured $^{3}J_{HN\alpha}$ coupling constants follow the predicted ones closely (Figure 3A). The αIIb tail behaves as expected for a random-coil peptide. Also, no helical tendency is propagated from the coiled-coil into the tail. The β3 tail, on the other hand, contains two major regions that deviate from random-coil (Figure 3B). Residues Arg^{724}−Ala^{735} exhibit lower than random-coil $^{3}J_{HN\alpha}$ coupling constants, indicating helical propensity. This region also has the highest NOE values of tail residues and a low hydrophobicity, indicating the existence of transient structure. Residues Asn^{744}−Tyr^{747}, the NPLY sequence motif (*59*, *60*), and adjacent residues also have relatively high NOE values. NPLY has been reported to possess a tendency to adopt reverse-turn (type I β-turn) conformations (*61*), and the observed coupling constants suggest slightly extended conformations for Asn^{744} and Tyr^{747} in agreement with β-turn conformations (Pro^{745} does not have an H^N signal and a coupling constant for Leu^{746} could not be determined due to spectral overlap). Residues Leu^{718}−Thr^{720} also deviate from random-coil exhibiting extended conformations, but also high hydrophobicities. Thus, although globally unfolded the β3

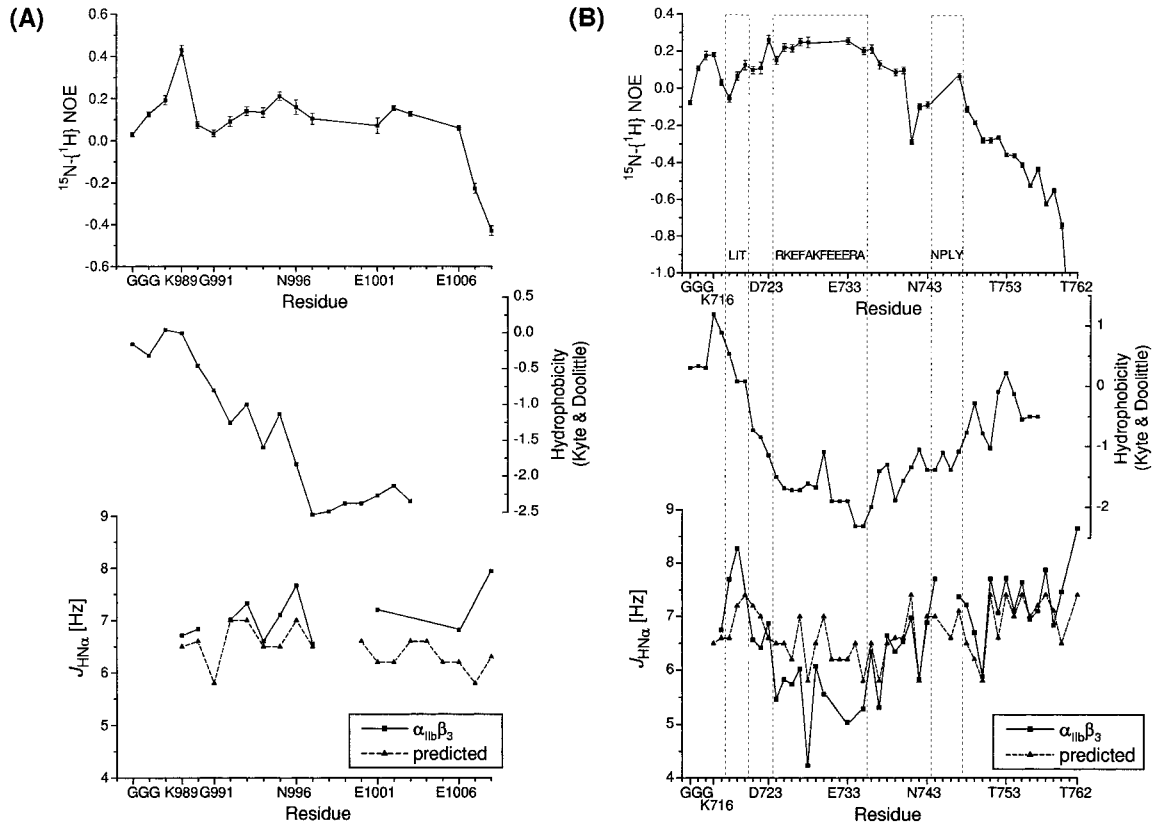

FIGURE 3: Structural and dynamical properties of the (A) αIIb and (B) β3 tails in the $(Gly)_3$-linked αIIbβ3 construct (Table 2a,b) in 10 mM acetic acid-d_3 pH 4.5, 37 °C. The coiled-coil is no longer shown. The ^{15}N-{^{1}H} NOE, hydrophobicities, and $^{3}J_{HN\alpha}$ coupling constants for each amino acid residue are compared for each tail. The experimentally obtained $^{3}J_{HN\alpha}$ coupling constants are also compared to those predicted theoretically to determine regions, which deviate from random-coil (shown boxed). Because of signal overlap, parameters could not be obtained for all residues. The αIIb tail behaves as expected for random-coil, while the β3 tail exhibits two distinct regions that deviate from random-coil, namely, residues Arg^{724}−Ala^{735} and Asn^{744}−Tyr^{747}. Residues Arg^{724}−Ala^{735} exhibit helical tendencies; residues Asn^{744}−Tyr^{747}, the NPLY sequence motif (*59, 60*), are likely to adopt reverse-turn conformations, which are characteristic for NPXY sequence motifs (*61*). Residues Leu^{718}−Thr^{720} also deviate from random-coil exhibiting extended conformations, but also high hydrophobicities.

tail possesses two regions that exhibit distinct transient structure.

Disruption of β3 Tail Structure and Function by Disruption of the NPXY Motif. Most integrin β cytoplasmic domains contain one or two NPXY motifs that are critical to their functions (*2, 6*). For example, changing a Tyr in the first "NPXY" motif of β3 to an Ala (β3(Y747A)) (*11, 20, 62*) causes reduced targeting of β3-containing integrins to cytoskeletal structures and a suppression of bidirectional signaling. Furthermore, a mutation in an NPXY motif in β1A (β1A(Y788A)) has similar biological effects and blocks the binding of the cytoskeletal proteins talin and filamin (*32*). As discussed above, the NPLY motif within the β3 tail context is likely to form a reverse-turn that might be disrupted by the Y747A mutation. Consequently, we analyzed the effects of this mutation in the β3 tail.

To analyze the β3 tail in the absence of αIIb, we compared the properties of a JG3αT-FG3β3 and JG3αT-FG3β3-(Y747A) model proteins. As will be discussed later in detail, the unpaired β3 tail exhibits essentially the same structural and dynamic properties as the αIIb paired β3 tail within the context of the coiled-coil (JG3αIIb-FG3β3). Affinity chromatography was used to quantify the interaction of the talin head domain (talin residues 1−435) with the β3 tail model proteins. Talin bound to JG3αT-FG3β3 tightly (EC50 = 134 nM) and saturably (Figure 4). In sharp contrast, the Y747A mutation reduced talin binding to undetectable levels. Thus, the Y747A mutation reduces β3's affinity for the talin head domain by more than an order of magnitude.

The functional effects of the Y747A mutation were associated with a dramatic structural change. The NPLY reverse-turn forming motif (*61*) was disrupted by substituting Ala for Tyr^{747} probably because of removal of the interaction between the aromatic side-chain of Tyr^{747} and the side chain of Asn^{744} (*61*). Observed changes in NMR parameters ($^{1}H^{N}$, ^{15}N chemical shifts, $^{3}J_{HN\alpha}$ coupling constants, and ^{15}N-{^{1}H} NOEs) of the mutant β3 model protein (Table 2i) as compared to the wild type β3 model protein (Table 2c) suggest that the mutation leads to the loss of reverse-turn propensity (and also confirms its prior presence). The relatively high NOEs of residues Ala^{742}−Ala^{750} are reduced, now descending almost linearly from Arg^{736} toward the C-terminus (Figure 5A). The absence of the structural integrity of the reverse turn also appears to destabilize the helical region somewhat (residues Arg^{724}−Ala^{735}). The observed chemical shift perturbations (Figure 5C,D) correlate well with the NOE data. Large changes were observed for both $^{1}H^{N}$ and ^{15}N shifts of residues Ala^{742}−Ala^{750} and small changes for the ^{15}N shifts of residues Lys^{716}−Thr^{741}. The large shift changes observed for Lys^{748} is a direct consequence of mutating the preceding residue (*52*). The relatively large changes for residues Ala^{742}−Ala^{750} reflect the loss of the reverse turn propensity as well as the Y747A substitution. The change of the $^{3}J_{HNHa}$ coupling constants between the

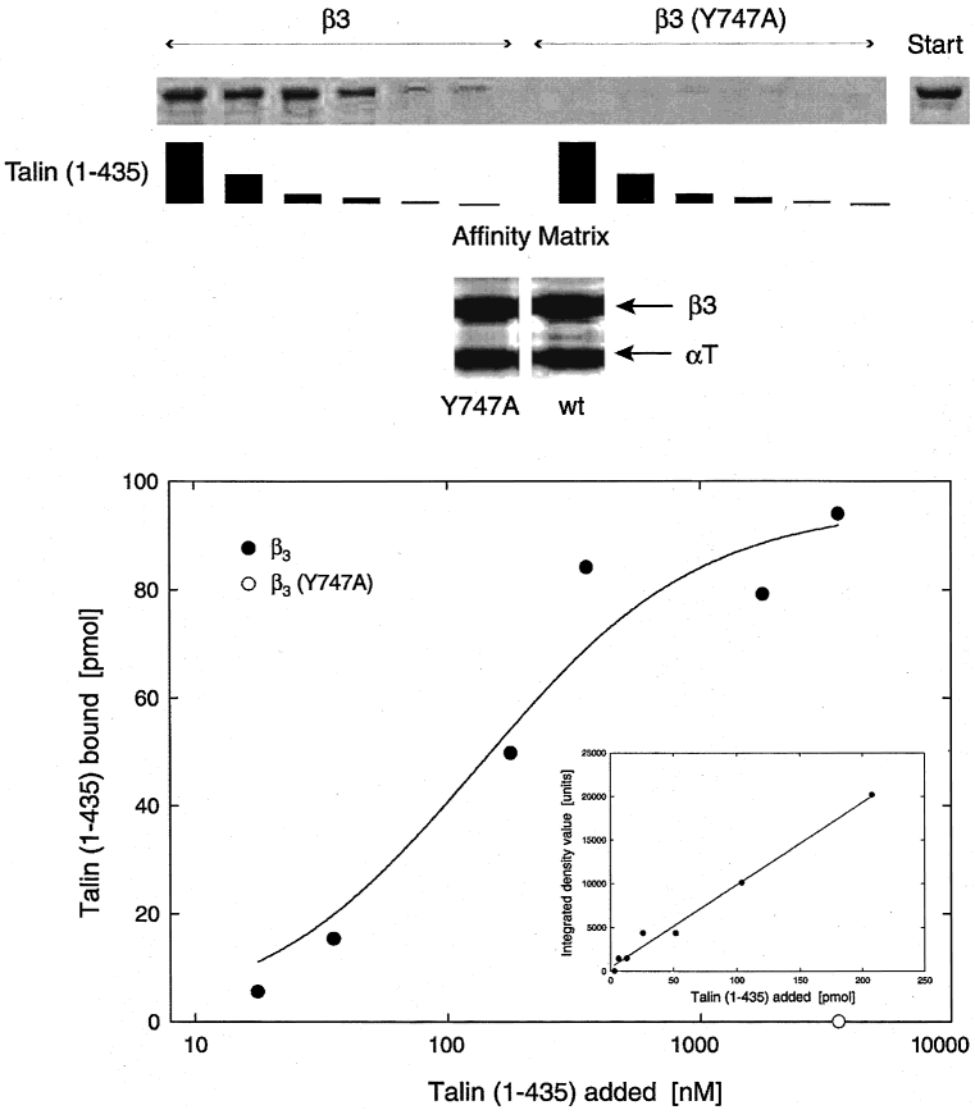

FIGURE 4: Inhibition of binding of the talin head domain to β3(Y747A). JG3αT-FG3β3 and JG3αT-FG3β3(Y747A) model proteins were immobilized on His-Bind Ni^{2+} chelate resin. Varying concentrations of a glutathione *S*-transferase (GST) recombinant talin head domain (residues 1−435 of talin) (*49*) were added to 100 μL of a 5% slurry of the model protein-coated resin. After 1 h incubation at room temperature, with continuous shaking, the resin was washed and bound proteins were eluted and analyzed by 4−20% SDS−PAGE under reducing conditions. Bound talin head domain was visualized by and quantified by scanning densitometry. The upper panel depicts Coomassie Blue staining of the talin bound to JG3αT-FG3β3 (β3) or JG3αT-FG3β3(Y747A) (β3(Y747A)) model proteins and the starting material. The middle panel depicts Coomassie Blue staining of each model protein bound to the resin and confirms the equal loading of JG3αT-FG3β3 and JG3αT-FG3β3(Y747A) model proteins. The positions of each mini-subunit is indicated. The bottom panel depicts the quantification of talin binding to each mini-subunit. Note the absence of binding to JG3αT-FG3β3(Y747A) model protein. The inset depicts the standard curve for density of the talin Coomassie Blue stained band versus talin head domain added. Note that all measurements were in the linear portion of the standard curve.

two forms is much less pronounced (Figure 5B). Although the whole NPLY motif has been disrupted, only the coupling constant of residue 747 changes significantly. Ala has intrinsically a low coupling constant (predicted 5.8 Hz) due to its high helix-forming propensity (*54*). This probably shows that a relatively small percentage of conformers were adopting reverse-turn conformations. Nevertheless, substituting Tyr^{747} with Ala and concomitant disruption of this reverse-turn is associated with profound loss of function of the β3 tail.

Helix Propagation into the β3 Tail. In the intact integrin receptor, helix could be propagated from the transmembrane helices into the tails. To estimate of the range of helix propagation into β3, the $^1H^N$, ^{15}N chemical shifts of β3 of the $(Gly)_3$-linker free αIIbβ3 construct (Table 2h) were compared to the αIIbβ3 construct with the $(Gly)_3$-linker (Table 2a).

The transition between the coiled-coil and the β3 tail becomes less abrupt. The first few tail residues in the linker-free construct have a much lower signal intensity than those with the $(Gly)_3$ linker (data not shown) and residues Lys^{716}−Ile^{719} could not be assigned unambiguously as these residues were obscured by more intense tail residues. The first eight residues of the β3 tail (Lys^{716}−Asp^{723}) are directly affected by helix propagation (Figure 6). Residues Lys^{725}−Arg^{734} are indirectly affected, probably by a slight stabilization of the helical nature of this region through the reduced mobility of the preceding residues rather than helix-propagation from the coiled-coil.

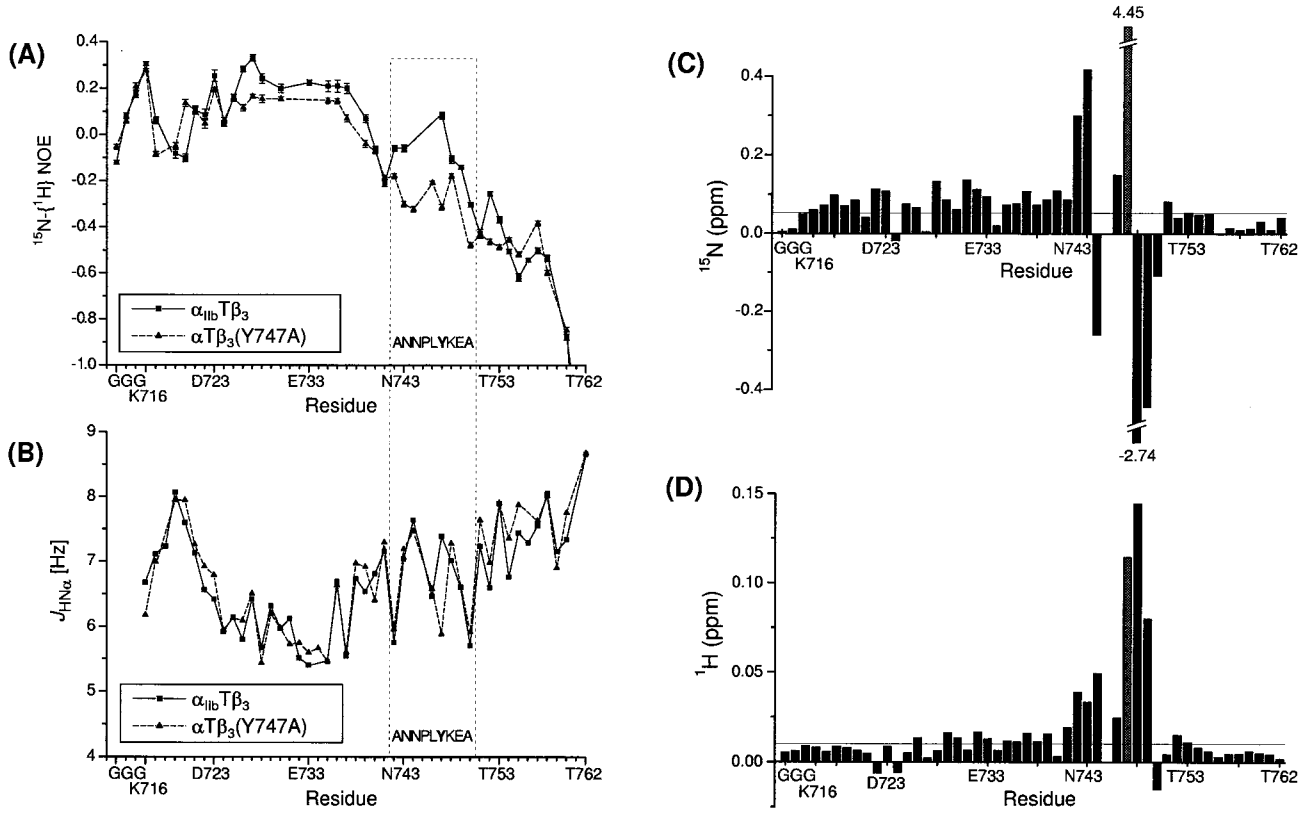

FIGURE 5: Comparison of the (A) ^{15}N-{^{1}H} NOEs, (B) $^{3}J_{HN\alpha}$ coupling constants, (C) ^{15}N and (D) $^{1}H^{N}$ chemical shifts differences of the $(Gly)_3$-linked, alpha tail truncated (αT) wild-type β3 and β3(Y747A) constructs ^{15}N labeled on β3 (Table 2c,i) in 10 mM acetic acid-d_3 pH 4.5, 37 °C. The error is ± 0.05 ppm for ^{15}N and ± 0.01 ppm for $^{1}H^{N}$ shifts. The observed differences indicate that the mutation disrupts the structural integrity of the NPLY motif.

Tail−Tail Interactions. NMR parameters ($^{1}H^{N}$, ^{15}N chemical shifts, $^{3}J_{HN\alpha}$ coupling constants, ^{15}N-{^{1}H} NOEs and, in some cases, ^{15}N T_2 relaxation times) observed for various constructs were compared. The different constructs correspond essentially to monomeric (Table 2c,d), heterodimeric (Table 2a,b), and homodimeric (Table 2e,f) tails, so that observed differences in NMR parameters are expected to be a very sensitive indicator of specific interactions between αIIb and β3. In all cases, however, these parameters were very similar (see Supplementary Information) indicating that the αIIb and β3 tails have undetectable interactions with each other in the context of the coiled-coil construct. Constructs with different lengths of the glycine linker (Table 2j−m, resulting in relative vertical tail−tail shifts of −2 to +2 residues) and the presence of divalent cations (5 mM Ca^{2+}) did not significantly change this behavior. Upon addition of Ca^{2+} small chemical shift changes in the acidic αIIb stretch EEDDEE (residues 1001−1006) were observed (data not shown), suggesting a divalent cation interaction in this region, as reported in ref *27*.

The interaction of free αIIb peptide with β3 attached to the coiled-coil via the $(Gly)_3$ linker (Table 2g) was also studied. This should allow αIIb to interact with β3 in all possible orientations. The $^{1}H^{N}$, ^{15}N chemical shifts of β3 were compared in the absence and presence of αIIb peptide at pH 7.4 and 6.8, in the presence of 5 mM Ca^{2+}, and were found to be very similar (Figure 7). This particular system (free αIIb peptide with β3 attached to the coiled-coil via the $(Gly)_3$ linker) was further studied at pH 7.4, in the presence of 5 mM Ca^{2+} by isothermal titration calorimetry (ITC). With the experiment set up to detect interactions in the micromolar range, no significant enthalpy changes could be detected (data not shown).

DISCUSSION

We have shown that the αIIb and β3 tails, fused to a coiled-coil, are suitable for NMR studies. Helix propagation, from the coiled-coil into the tails, can be eliminated by a $(Gly)_3$ linker between the coiled-coil and the tails, but omission of this linker leads to significant helix propagation into β3. The vertical stagger of the two tails can also be adjusted by varying the linker length. Some horizontal freedom for the adjacent tails at the C-terminus of the coiled-coil is provided by the flexible nature of the $(Gly)_3$ linker.

In aqueous solution, the αIIb and β3 tails are largely unstructured, although part of the β3 tail has a propensity to form a helix (residues Arg^{724}−Ala^{735}) and part (the NPLY motif) has a tendency to form a β-turn. The structural propensity of the NPLY motif (Asn^{744}−Tyr^{747}) is collapsed by the mutation Y747A, which also markedly reduces the affinity of the head domain of the cytoskeletal protein, talin (*49*) for β3. Surprisingly, no significant interactions between the αIIb and β3 tails could be detected within the context of our constructs.

A detailed study of the $^{3}J_{HN\alpha}$ coupling constants and ^{15}N-{^{1}H} NOEs of most residues has shown that the $(Gly)_3$ linker is flexible. Furthermore, the αIIb tail behaves as random-coil, while the β3 tail exhibits two transiently structured regions. This is in agreement with reported CD studies of the tails, which have indicated a random-coil αIIb tail and a small amount of secondary structure in the β3 tail (*26*, *27*).

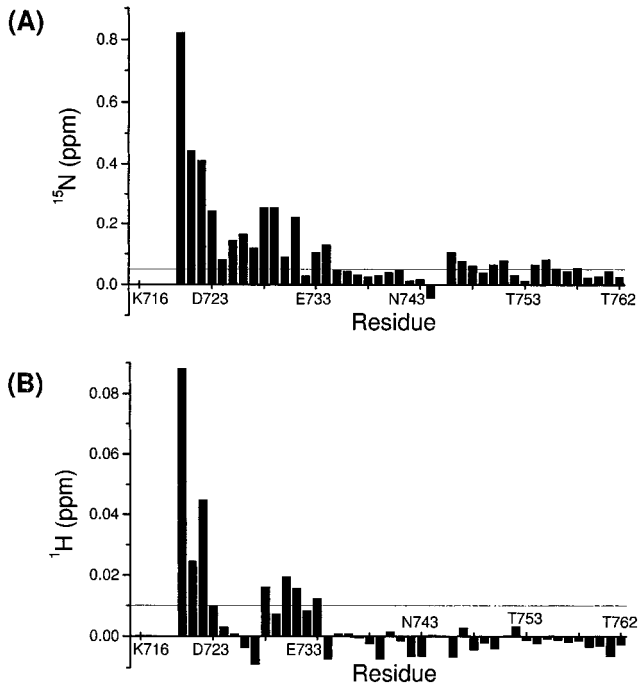

FIGURE 6: (A) ^{15}N and (B) $^{1}H^{N}$ chemical shift differences between the $(Gly)_3$-linked (Table 2a) and $(Gly)_3$-free αIIbβ3 constructs (Table 2h) in 10 mM acetic acid-d_3 pH 4.5, 37 °C. The error is ± 0.05 ppm for ^{15}N and ± 0.01 ppm for $^{1}H^{N}$ shifts. Residues Lys^{716}−Ile^{719} could not be assigned unambiguously in the $(Gly)_3$-free αIIbβ3 construct (Table 2h), and no values are shown for these residues. The observed differences arise from helix propagation from the coiled-coil into the integrin tails.

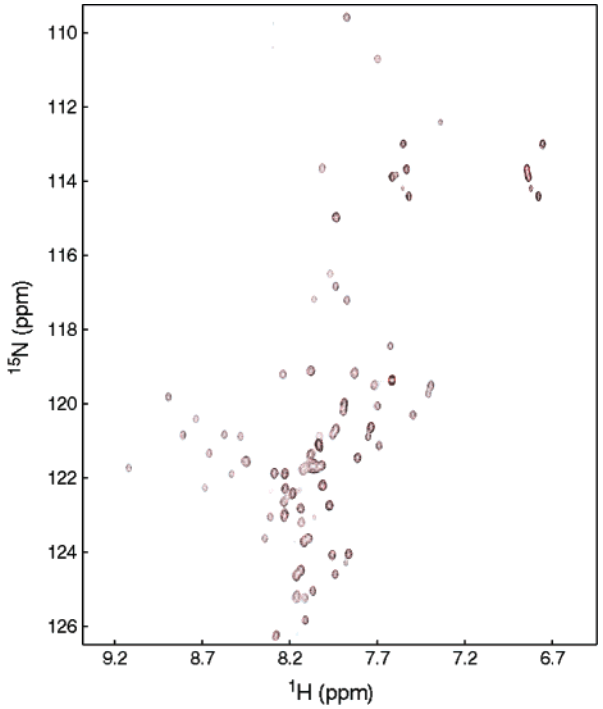

FIGURE 7: Superposition of $^{1}H^{N}$-^{15}N correlation (HSQC) spectra of 0.6 mM J, FG3β3 model protein (Table 2g) in 50 mM Tris-d_{11}/HCl pH 6.8, 100 mM NaCl, 5 mM $CaCl_2$ in the absence (black signals) and presence (red signals) of 1.2 mM free αIIb peptide at 30 °C and 600 MHz. No significant chemical shift changes occurred, suggesting that the free αIIb peptide does not interact with J, FG3β3. Because of much faster amide proton chemical exchange with solvent water the signal intensities are now very different from the situation at pH 4.5 (Figure 2). The signals arising from the $(Gly)_3$ linker have almost completely disappeared.

The amount of helix propagation that can be introduced into the β3 tail and might be present after the transmembrane helix in vivo was tested. Pronounced effects, as judged from $^{1}H^{N}$, ^{15}N shift differences observed on omission of the $(Gly)_3$ linker connecting the coiled-coil and β3 tail, were observed for up to eight residues (Lys^{716}−Asp^{723}). Smaller effects also occur within the helical region of β3 (residues Arg^{724}−Ala^{735}), probably arising from a slight helix stabilization, through the reduced mobility of the preceding residues. Some studies have suggested that αIIb(Lys^{989}−Phe^{993}) and β3-(Lys^{716}−Ile^{721}) are within the transmembrane region (*63*−*65*). If this were the case, it would be expected that the helical content of the region of the β3 tail would increase. Helix propagation into the αIIb tail is probably less significant due to the presence of Pro^{998} and Pro^{999}. Detailed structural information about the tails has so far only been reported for the αIIb tail in nonaqueous or DPC micelle solution. It has been reported that in 45% TFE solution the αIIb peptide adopts a defined, mostly helical, structure (*31*). Myristoylated αIIb in DPC micelle solution has also been reported to adopt a defined, mostly helical, structure (*30*). Our results indicate that no helix forms intrinsically in aqueous solution, but as our experiments were carried out in the absence of membrane we clearly cannot rule out in vivo αIIb tail/membrane interactions. The study of myristoylated αIIb in DPC micelle solution (*30*) points toward a possible important role of a phospholipid layer in inducing defined structure in the αIIb tail.

We have compared the $^{3}J_{HN\alpha}$ coupling constants, ^{15}N-{^{1}H} NOEs, $^{1}H^{N}$ and ^{15}N chemical shifts between the wild-type β3 and β3(Y747A). Our results suggest that Y747A disrupts the structural integrity of the NPLY motif and greatly reduces the affinity of the head domain of talin for β3. The helical region (residues Arg^{724}−Ala^{735}) also appears to be somewhat destabilized by the absence of the reverse-turn tendency. The mutation Y747A is known to lock integrin αIIbβ3 receptor in its resting state (*11*, *66*). Hence, it can be speculated that the ligand, which occupies the NPLY motif, e.g., talin, is involved in integrin αIIbβ3 activation.

Reported in vitro interactions between the αIIb and β3 tails derived from qualitative analysis of CD and/or intrinsic fluorescence (*26*, *27*) upon mixing both tails and from quantitative analysis of surface plasmon resonance in the micromolar affinity range of immobilized GST-β3 and free αIIb peptide (*29*) could not be confirmed here. We could not detect significant changes of $^{3}J_{HN\alpha}$ coupling constants, ^{15}N-{^{1}H} NOEs, $^{1}H^{N}$ and ^{15}N chemical shifts between differently paired tails indicative of a specific interaction between the αIIb and β3 tails fused to the coiled-coil. We were also unable to detect significant $^{1}H^{N}$, ^{15}N chemical shift or enthalpy changes upon mixing free αIIb peptide with β3 fused to the coiled-coil. These differences might stem from the different constructs used to study the integrin tails. In the present study, β3 is always within the context of the coiled-coil construct. We have shown that we can separate the structural properties of the helix and the tail. Nevertheless, we cannot absolutely exclude the possibility that some constraint in the coiled-coil construct limits the interaction of the tails.

The situation in vivo is complicated by the existence of

multiple potential ligands for the tails of integrin αIIbβ3 (*67*). Our in vitro results and the apparent direct, specific interaction between αIIb and β3 in vivo (*25*) suggest that, in vivo, interactions might occur on the surface of another factor (e.g., another protein or the lipid bilayer). Binding of factors to the integrin tails may cause their local structure to change, but this may not be transmitted through the membrane and hence, not cause signaling. Alternatively, transitions between the resting and active state (*66*) could be induced by changes in ternary or higher order complexes of tails and factor(s). Activation of integrin αIIbβ3 could occur by alterations of the relative orientation of the transmembrane helices by the association/dissociation of the factor(s) from the integrin tails. The helical tendency of β3 residues Arg^{724}−Ala^{735} might represent another important motif for ligand binding and for the regulation of the affinity state of integrin αIIbβ3. Indeed, this region has also been implicated in talin binding (*68*) and α-actinin binds to a similar region in the β1A tail (*69*). Furthermore, the slight destabilization of this region through the effects of the Y747A mutation could also contribute to reduced talin binding to the β3 tail.

ACKNOWLEDGMENT

Helpful discussions with Jonathan Boyd, Lorna Smith, and David Staunton are appreciated.

SUPPORTING INFORMATION AVAILABLE

Two figures comparing the $^1H^N$, ^{15}N chemical shifts, $^3J_{HN\alpha}$ coupling constants and ^{15}N-{^1H} NOEs of the constructs depicted in Table 2a,b with Table 2c,d and Table 2e,f. This material is available free of charge via the Internet at http://pubs.acs.org.

REFERENCES

1. Hynes, R. O. (1992) *Cell 69*, 11−25.
2. Sastry, S. K., and Horwitz, A. F. (1993) *Curr. Opin. Cell Biol. 5*, 819−831.
3. Schwartz, M. A., Schaller, M. D., and Ginsberg, M. H. (1995) *Annu. Rev. Cell Dev. Biol. 11*, 549−599.
4. Dedhar, S., and Hannigan, G. E. (1996) *Curr. Opin. Cell Biol. 8*, 657−669.
5. Hemler, M. E. (1998) *Curr. Opin. Cell Biol. 10*, 578−585.
6. Liu, S. C., Calderwood, D. A., and Ginsberg, M. H. (2000) *J. Cell Sci. 113*, 3563−3571.
7. Hayashi, Y., Haimovich, B., Reszka, A., Boettiger, D., and Horwitz, A. (1990) *J. Cell Biol. 110*, 175−184.
8. Reszka, A. A., Hayashi, Y., and Horwitz, A. F. (1992) *J. Cell Biol. 117*, 1321−1330.
9. Hibbs, M. L., Xu, H., Stacker, S. A., and Springer, T. A. (1991) *Science 251*, 1611−1613.
10. Hughes, P. E., Otoole, T. E., Ylanne, J., Shattil, S. J., and Ginsberg, M. H. (1995) *J. Biol. Chem. 270*, 12411−12417.
11. Otoole, T. E., Ylanne, J., and Culley, B. M. (1995) *J. Biol. Chem. 270*, 8553−8558.
12. Otoole, T. E., Katagiri, Y., Faull, R. J., Peter, K., Tamura, R., Quaranta, V., Loftus, J. C., Shattil, S. J., and Ginsberg, M. H. (1994) *J. Cell Biol. 124*, 1047−1059.
13. Ylanne, J., Chen, Y., Otoole, T. E., Loftus, J. C., Takada, Y., and Ginsberg, M. H. (1993) *J. Cell Biol. 122*, 223−233.
14. Otoole, T. E., Mandelman, D., Forsyth, J., Shattil, S. J., Plow, E. F., and Ginsberg, M. H. (1991) *Science 254*, 845−847.
15. Crowe, D. T., Chiu, H., Fong, S., and Weissman, I. L. (1994) *J. Biol. Chem. 269*, 14411−14418.
16. Chen, Y. P., Otoole, T. E., Shipley, T., Forsyth, J., Laflamme, S. E., Yamada, K. M., Shattil, S. J., and Ginsberg, M. H. (1994) *J. Biol. Chem. 269*, 18307−18310.
17. Laflamme, S. E., Thomas, L. A., Yamada, S. S., and Yamada, K. M. (1994) *J. Cell Biol. 126*, 1287−1298.
18. Lukashev, M. E., Sheppard, D., and Pytela, R. (1994) *J. Biol. Chem. 269*, 18311−18314.
19. Mastrangelo, A. M., Homan, S. M., Humphries, M. J., and LaFlamme, S. E. (1999) *J. Cell Sci. 112*, 217−229.
20. Tahiliani, P. D., Singh, L., Auer, K. L., and LaFlamme, S. E. (1997) *J. Biol. Chem. 272*, 7892−7898.
21. Leong, L., Hughes, P. E., Schwartz, M. A., Ginsberg, M. H., and Shattil, S. J. (1995) *J. Cell Sci. 108*, 3817−3825.
22. Yauch, R. L., Felsenfeld, D. P., Kraeft, S. K., Chen, L. B., Sheetz, M. P., and Hemler, M. E. (1997) *J. Exp. Med. 186*, 1347−1355.
23. Kassner, P. D., Kawaguchi, S., and Hemler, M. E. (1994) *J. Biol. Chem. 269*, 19859−19867.
24. Filardo, E. J., and Cheresh, D. A. (1994) *J. Biol. Chem. 269*, 4641−4647.
25. Hughes, P. E., DiazGonzalez, F., Leong, L., Wu, C. Y., McDonald, J. A., Shattil, S. J., and Ginsberg, M. H. (1996) *J. Biol. Chem. 271*, 6571−6574.
26. Muir, T. W., Williams, M. J., Ginsberg, M. H., and Kent, S. B. H. (1994) *Biochemistry 33*, 7701−7708.
27. Haas, T. A., and Plow, E. F. (1996) *J. Biol. Chem. 271*, 6017−6026.
28. Haas, T. A., and Plow, E. F. (1997) *Protein Eng. 10*, 1395−1405.
29. Vallar, L., Melchior, C., Plancon, S., Drobecq, H., Lippens, G., Regnault, V., and Kieffer, N. (1999) *J. Biol. Chem. 274*, 17257−17266.
30. Vinogradova, O., Haas, T., Plow, E. F., and Qin, J. (2000) *Proc. Natl. Acad. Sci. U.S.A. 97*, 1450−1455.
31. Hwang, P. M., and Vogel, H. J. (2000) *J. Mol. Recognit. 13*, 83−92.
32. Pfaff, M., Liu, S. C., Erle, D. J., and Ginsberg, M. H. (1998) *J. Biol. Chem. 273*, 6104−6109.
33. John, M., Briand, J. P., Grangerschnarr, M., and Schnarr, M. (1994) *J. Biol. Chem. 269*, 16247−16253.
34. Calvete, J. J., Schafer, W., Henschen, A., and Gonzalezrodriguez, J. (1990) *FEBS Lett. 272*, 37−40.
35. Boyd, J., Soffe, N., John, B., Plant, D., and Hurd, R. (1992) *J. Magn. Reson. 98*, 660−664.
36. Grzesiek, S., and Bax, A. (1993) *J. Am. Chem. Soc. 115*, 12593−12594.
37. Marion, D., Driscoll, P. C., Kay, L. E., Wingfield, P. T., Bax, A., Gronenborn, A. M., and Clore, G. M. (1989) *Biochemistry 28*, 6150−6156.
38. Driscoll, P. C., Clore, G. M., Marion, D., Wingfield, P. T., and Gronenborn, A. M. (1990) *Biochemistry 29*, 3542−3556.
39. Jahnke, W., Baur, M., Gemmecker, G., and Kessler, H. (1995) *J. Magn. Reson. Ser. B 106*, 86−88.
40. Bartels, C., Xia, T. H., Billeter, M., Guntert, P., and Wuthrich, K. (1995) *J. Biomol. NMR 6*, 1−10.
41. Farrow, N. A., Zhang, O. W., Formankay, J. D., and Kay, L. E. (1994) *J. Biomol. NMR 4*, 727−734.
42. Kay, L. E., Torchia, D. A., and Bax, A. (1989) *Biochemistry 28*, 8972−8979.
43. Boyd, J., Hommel, U., and Krishnan, V. V. (1991) *Chem. Phys. Lett. 187*, 317−324.
44. Palmer, A. G., Skelton, N. J., Chazin, W. J., Wright, P. E., and Rance, M. (1992) *Mol. Phys. 75*, 699−711.
45. Palmer, A. G., Rance, M., and Wright, P. E. (1991) *J. Am. Chem. Soc. 113*, 4371−4380.
46. Kay, L. E., Brooks, B., Sparks, S. W., Torchia, D. A., and Bax, A. (1989) *J. Am. Chem. Soc. 111*, 5488−5490.
47. Kay, L. E., and Bax, A. (1990) *J. Magn. Reson. 86*, 110−126.
48. Redfield, C., Smith, L. J., Boyd, J., Lawrence, G. M. P., Edwards, R. G., Smith, R. A. G., and Dobson, C. M. (1991) *Biochemistry 30*, 11029−11033.
49. Calderwood, D. A., Zent, R., Grant, R., Rees, D. J. G., Hynes, R. O., and Ginsberg, M. H. (1999) *J. Biol. Chem. 274*, 28071−28074.
50. Wüthrich, K. (1986) *NMR of Proteins and Nucleic Acids*, John Wiley & Sons, Inc., New York.

51. Bracken, C., Carr, P. A., Cavanagh, J., and Palmer, A. G. (1999) *J. Mol. Biol. 285*, 2133-2146.
52. Braun, D., Wider, G., and Wuthrich, K. (1994) *J. Am. Chem. Soc. 116*, 8466−8469.
53. Dedios, A. C., Pearson, J. G., and Oldfield, E. (1993) *Science 260*, 1491−1496.
54. Fersht, A. (1999) *Structure and Mechanism in Protein Science*, W. H. Freeman & Company, New York.
55. Penkett, C. J., Redfield, C., Dodd, I., Hubbard, J., McBay, D. L., Mossakowska, D. E., Smith, R. A. G., Dobson, C. M., and Smith, L. J. (1997) *J. Mol. Biol. 274*, 152−159.
56. Smith, L. J., Fiebig, K. M., Schwalbe, H., and Dobson, C. M. (1996) *Fold. Des. 1*, R95−R106.
57. Alexandrescu, A. T., and Shortle, D. (1994) *J. Mol. Biol. 242*, 527−546.
58. Kyte, J., and Doolittle, R. F. (1982) *J. Mol. Biol. 157*, 105−132.
59. Jing, S. Q., Spencer, T., Miller, K., Hopkins, C., and Trowbridge, I. S. (1990) *J. Cell Biol. 110*, 283−294.
60. Chen, W. J., Goldstein, J. L., and Brown, M. S. (1990) *J. Biol. Chem. 265*, 3116−3123.
61. Bansal, A., and Gierasch, L. M. (1991) *Cell 67*, 1195−1201.
62. Ylanne, J., Huuskonen, J., Otoole, T. E., Ginsberg, M. H., Virtanen, I., and Gahmberg, C. G. (1995) *J. Biol. Chem. 270*, 9550−9557.
63. Armulik, A., Nilsson, I., von Heijne, G., and Johansson, S. (1999) *J. Biol. Chem. 274*, 37030−37034.
64. Poncz, M., Eisman, R., Heidenreich, R., Silver, S. M., Vilaire, G., Surrey, S., Schwartz, E., and Bennett, J. S. (1987) *J. Biol. Chem. 262*, 8476−8482.
65. Fitzgerald, L. A., Steiner, B., Rall, S. C., Lo, S. S., and Phillips, D. R. (1987) *J. Biol. Chem. 262*, 3936−3939.
66. Yan, B., Hu, D. D., Knowles, S. K., and Smith, J. W. (2000) *J. Biol. Chem. 275*, 7249−7260.
67. Hughes, P. E., and Pfaff, M. (1998) *Trends Cell Biol. 8*, 359−364.
68. Patil, S., Jedsadayanmata, A., Wencel-Drake, J. D., Wang, W., Knezevic, I., and Lam, S. C. T. (1999) *J. Biol. Chem. 274*, 28575−28583.
69. Otey, C. A., Vasquez, G. B., Burridge, K., and Erickson, B. W. (1993) *J. Biol. Chem. 268*, 21193-21197.
70. Oshea, E. K., Klemm, J. D., Kim, P. S., and Alber, T. (1991) *Science 254*, 539−544.

BI010338L